Journal of Chemical Health Risks

www.jchr.org

JCHR (2025) 15(5), 904-920 | ISSN:2251-6727

# Design and Assessment of PLGA based Tetrandrine Nanoparticles for Intranasal delivery targeting for Glioblastoma

**Neha Binjhade, Suchitra S. Mishra*, Ujwala Mahajan**

Dadasaheb Balpande College of Pharmacy, Besa, Nagpur, MS,440037, India

***Corresponding Author**

Dr. Suchitra Mishra, Assistant Professor, Pharmaceutics Department, Dadasaheb Balpande College of Pharmacy, Nagpur, MH,440037, India.

***Received Date: 15/07/2025*** ***Revised Date: 10/08/2025*** ***Accepted Date: 08/09/2025***

**KEYWORDS**

Glioblastoma multiforme, malignant, tetrandrine, Box–Behnken design, drug–polymer interaction

**ABSTRACT:**

Glioblastoma multiforme represents a malignant brain tumor characterized by poor treatment availability. This study aimed to enhance nasal-to-brain delivery of tetrandrine, a bisbenzylisoquinoline alkaloid with anticancer potential, by formulating poly(lactic-co-glycolic acid) (PLGA) nanoparticles incorporated into a thermosensitive in situ gel (poloxamer 407). Nanoparticles were optimized via Box–Behnken design and characterized for physicochemical properties, exhibiting 169– 846 nm particle size, -31.9 to -19.9 mV zeta potential, high entrapment efficiency, and spherical morphology. FTIR, DSC, and XRD confirmed no drug–polymer interaction. The in situ gel showed suitable gelation temperature, pH, viscosity, and sustained in vitro release, with nanoparticle-loaded gel achieving prolonged drug release compared to plain drug gel. Ex vivo permeation across goat nasal mucosa demonstrated superior permeation for nanoparticle formulations. Cytocompatibility and hemolysis studies indicated good biocompatibility. These findings suggest PLGA nanoparticle–loaded in situ gel as a promising nasal delivery system for sustained tetrandrine release and potential improvement in glioblastoma therapy.

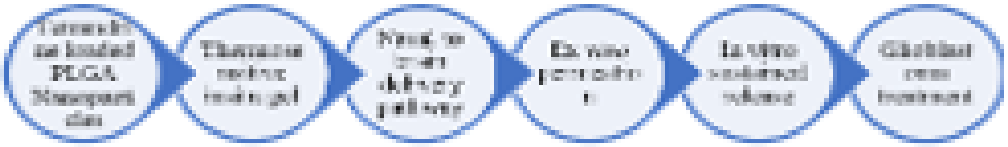

**Figure 1- Graphical Abstract**

## INTRODUCTION

Gliomas represent the most prevalent type of initial cerebral tumors, and average endurance duration for patient with GBMis approximately 9 months [22,23]. Surgery is the primary treatment option for gliomas; however, due to their invasive nature, complete surgical removal is not possible [24]. Chemotherapy plays an increasingly vital role in treatment following glioma resection. An increasing body of research has explored the anti-tumor effects of TET. It promotes cancer cell apoptosis by initiating a ROS-dependent mitochondrial pathway, facilitating the discharge of cytochrome c from mitochondria, triggering caspases-3, -8, and -9, inducing PARP fragmentation, and lowering Bcl-XL expression [25, 26,27]. In most tumor cells, TET leads to cell cycle arrest at the G0/G1 phase [28]. Additionally, TET has been shown to modulate pro-angiogenic protein under in vitro conditions, vascular lining growth elements and hypoxia- activated factor-1 alpha [29]

Tetrandrine (TET), a bisbenzylisoquinoline alkaloid, is obtained from the dried roots of the traditional Chinese

Journal of Chemical Health Risks

www.jchr.org

JCHR (2025) 15(5), 904-920 | ISSN:2251-6727

medicinal herb*Stephania tetrandra* S. Moore [1] as well as other related members of the Menispermaceae family [2]. It demonstrates anti-cancer potential both under laboratory conditions and in living organisms to combat several mortal malignancies, including breast , prostate , liver, lung, pancreatic, leukemia, gastric and colorectal cancer [3–9]. TET has been identified as a calcium-channel blocker and has shown therapeutic effects in silicosis, hypertension, inflammation, and cancer without notable toxicity [2]. In colon cancer cells, TET induced G1-phase cell cycle arrest [10], promoted mitochondria-dependent TET triggered in human gastric cancer BGC-823 cells [11] and induced autophagy I human breast cancer MDA-MB-231 cells by suppressing the P13K/AKT/m TOR pathway [12]. In addition , TET reduced the motility and invasiveness of human colon cancer SW620 cells through down regulation of NF κB and matrix metalloproteinase signaling mechanism [13]. In experimental models, TET also reduced glioma growth and angiogenesis in rats [14,15]. Additionally, it reversed drug resistance by regulating expression [16]. Importantly, TET has been reported to significantly enhance transport across BBB by suppressing P-glycoprotein activity, which is highly expressed at the BBB [17–19].

Tetrandrine is an anticancer drug that targets multiple signaling pathways involved in tumor progression and therapy resistance. It inhibits the Wnt/β-catenin pathway, downregulates STAT3, and induces reactive oxygen species (ROS) generation. It also suppresses the PI3K/Akt/mTOR pathway, reducing MMP2, MMP9, MDR2, and MRP1, leading to reduced angiogenesis, autophagy regulation, and decreased drug resistance as shown in figure 2. Additionally, it inhibits NF-κB signaling, sensitizing cancer cells to radiotherapy. These effects contribute to suppressing proliferation, apoptosis, angiogenesis inhibition, drug resistance reversal, and enhanced radiosensitivity. [20, 21]

Tetrandrine nasal to brain is a drug delivery method that uses the nasal cavity to reach the brain, bypassing the BBB. This method uses natural nasal pathways to transport the drug directly to the central nervous system. The olfactory nerve or trigeminal nerve supplies the nasal mucosa [30].Poly(lactic-co-glycolic acid) (PLGA) is an extensive researched polymer for nasal nanoparticle medication administration. PLGA is a combined polymer composed of polylactic acid (PLA) and polyglycolic acid (PGA) [31], where the proportion of each component determines its properties. PGA is a crystalline, hydrophilic polymer that degrades quickly, whereas PLA is hydrophobic with comparatively low mechanical stability. PLGA with a higher lactic acid content is more hydrophobic and exhibits a slight degradation rate because of numerous methyl substitute [32].

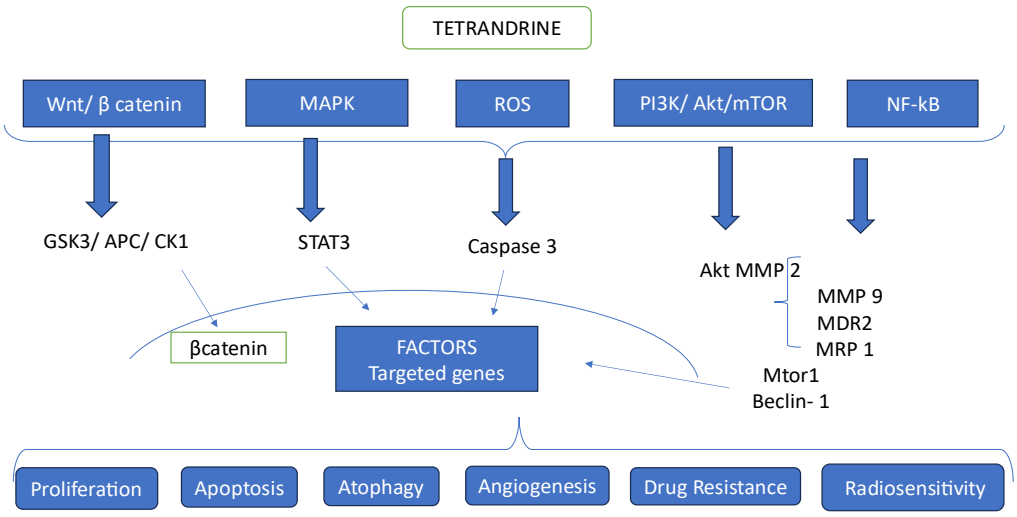


**Figure 2. Mechanism of Action of Tetrandrine**

Journal of Chemical Health Risks

www.jchr.org

JCHR (2025) 15(5), 904-920 | ISSN:2251-6727

PLGA is a decomposable polymer that gradually breakdown into the water-soluble units lactic acid (LA) and glycolic acid (GA) inside the body. These metabolites are further processed through the citric acid (Krebs) cycle and ultimately excreted as carbon dioxide and water. Being a bulk-eroding material, PLGA has gained regulatory approval from both the FDA and EMA for applications in pharmaceuticals and health care equipment. It is highly preferred for particulate nasal drug delivery, helping preventmedication deterioration within the nose passage and improving the encapsulation and administration of wide range of medications for differenttherapeutic purposes [33]

Tetrandrine-loaded nanoparticles were created produced employed a customized solvent displacement method [34,35]. The organic phase was prepared by dissolving tetrandrine and PLGA in acetone, while an aqueous phase was created by mixing ethanol and water with 0.1% Tween 80 [36]. The organic phase was slowly added to the aqueous phase, forming a milky colloidal suspension. The suspension was stirred at 900 rpm for 24 hours, adjusted with water, and left to stir overnight magnetically to remove any remaining organic phase. The formulation underwent sonication to reduce particle size to the desired range [37].

## MATERIALS AND METHODS

### Materials

Tetrandrine was procured from Tokyo Chemical Industry , Japan , and poly(lactic-co-glycolic acid) (PLGA; 50:50) was obtained fromMitsui Chemicals India, Pvt. Ltd. and all other analytical-grade solvents and chemicals were purchased from Loba Chemicals, India. Goat nasal mucosa was freshly obtained from a local slaughterhouse under hygienic conditions. Distilled water was used in all experiments.

### Formulation and Optimization of Tetrandrine-PLGA nanoparticles

A Box-Behnken statistical design (Design Expert® 13 software, Stat-Ease Inc., USA) was employed to optimize the formulation of tetrandrine-PLGA nanoparticles. This design assessed the impact of formulation attributes, including PLGA content (A), Tween 80 concentration (B), and drug ratio (C) on dependent parameters such as particle size (Y1), entrapment efficiency (Y2), and zeta potential (Y3) of the formulated batches were evaluated. A statistical design provided a series of predicted experimental runs, considering three autonomous parameters at their lower (−1), middle (0), and upper (+1) criteria of improvement of the nanoparticle formulation (Table 1). A program developed a quadratic equation applying a three factor, three stage experimental design, [41] targeting. International journal of pharmaceutics. 2020 Aug 30;586:119499.which is represented by the following equation:

**Table 1. Variables selected for Box-Behnken statistical design**

| Independent variables (Factors) | Variable levels | | | Dependent variables (Responses) |
|---|---|---|---|---|
| | Low(-1) | Medium (0) | High(+1) | |
| PLGA (mg) | 20 | 25 | 30 | Particle size (nm) |
| Tween (%) | 0.1% | 0.5% | 1% | Zeta Potential (mb) |
| Stirring Time (hr.) | 2 | 3 | 4 | Entrapment efficiency (%) |

### Characterization of Tetrandrine-PLGA nanoparticles

### Particle Size and Polydispersity Index

Dynamic light Scattering (DLS) was applied to mention particle dimensions and size distribution using a Zetasizer (Anton Paar). Approximately 1 mL of nanoparticle dispersion was diluted with double-distilled water and measured in a glass cuvette at 25 °C, with a detection angle of 173° backscatter (NIBS). The z- average particle size and PDI were calculated automatically by the instrument software, assuming

Journal of Chemical Health Risks

www.jchr.org

JCHR (2025) 15(5), 904-920 | ISSN:2251-6727

spherical geometry. Measurements were performed in triplicate [45]

**Zeta Potential**

The surface charge and dispersion stability of the nanoparticles were analyzed using a Litesizer 500 (Anton Paar) with an omega cuvette. A zeta potential value close to ±30 mV was considered indicative of good stability against aggregation and flocculation [44]

**Entrapment Efficiency (EE)**

The entrapment efficiency of tetrandrine-loaded PLGA nanoparticles was measured by centrifugal separation of Nanoparticle suspension at 6000 rpm for 30 minutes at 4 °C. The supernatant was diluted with phosphate buffer solutions (pH 5.5 and 6.8), and absorbance was measured at 236 nm using a UV spectrophotometer (UV-1800, Shimadzu, Japan). EE was calculated using the formula: [42,43]

Entrapment efficiency= $\frac{Total\ drug - Untrapped\ drug}{Total\ drug} \times 100$

**Fourier Transform Infrared Spectroscopy (FTIR)**
Functional groups and chemical interactions were examined using ATR-FTIR (NICOLET iS50, Thermo Fisher Scientific). Spectra of pure tetrandrine, tetrandrine-loaded PLGA nanoparticles, and physical mixtures were recorded in the range of 4000–400 $cm^{-1}$. Samples were prepared with potassium bromide (KBr), dried, and scanned in transmission mode [39]

**Differential Scanning Calorimetry (DSC)**
Thermal properties of pure tetrandrine and tetrandrine-loaded nanoparticles were analyzed using a DSC 214 Polyma (NETZSCH, Selb, Germany). Samples were prepared in ethanol at appropriate dilutions and scanned by UV spectrophotometry in the range of 200–400 nm [38].

**X-ray Diffraction (XRD)**
The crystalline nature of tetrandrine-loaded PLGA nanoparticles was characterized by XRD (Bruker AXS, Madison, WI, USA). The technique was used to detect polymorphic forms, crystal habit modifications, and new crystalline structures formed during nanoparticle synthesis [40].

**Field Emission Scanning Electron Microscopy (FE-SEM)**
Surface morphology of tetrandrine-loaded PLGA nanoparticles was examined using FE-SEM with SEM-EDAX (Jeol 6390LA/ OXFORD XMX N). Dried samples were imaged at various magnifications under an accelerating voltage of 15 kV to evaluate nanoparticle morphology and structural features.

**Formulation of *in – situ* gel**

The in situ gel was prepared using the cold method. Poloxamer 407 (24%w/w) was dispersed in distilled water at 4 °C under continuous stirring in an ice bath. Hydroxypropyl methylcellulose (HPMC K4M) was incorporated as a mucoadhesive agent. The solution was stored overnight in a refrigerator to ensure complete hydration, after which lactic acid was added to adjust the pH. The final gel formulation contained 1 mg of drug per 83 mg of gel and was stored under refrigerated conditions until further use[47]

**Evaluation of *in – situ* gel**

**Appearance**

The prepared tetrandrine in situ gel was visually inspected against white and black backgrounds to assess appearance, clarity, turbidity, and the presence of foreign particles.

**pH of gel**

The pH of the Gel was determined using a digital pHmeter (Elico Pvt. Ltd., India) by immersing the electrode directly into the formulation [48]

**Sol -Gel Transitions temperature (Tsol-Gel) and Gelation Formation Time**

The temperature of gelation was assessed by transferring 5 mL of the pre-gel formulation into a test tube submerged in a water bath with controlled thermal conditions. The bath temperature was gradually increased at a rate of 2 °C every 5 minutes with gentle shaking at intervals. The point at which the solution lost its fluidity was considered the gelation temperature, and the duration required for complete transformation from sol to gel was measured as the gelation duration [49].

Journal of Chemical Health Risks

www.jchr.org

JCHR (2025) 15(5), 904-920 | ISSN:2251-6727

**Viscosity**

Viscosity was measured for both the pre-gel solution and the formed gel using a Brookfield Cap Viscometer (Model 2000þ) at 25 °C and 37 °C, respectively. Measurements were performed in triplicate using spindle no. 3 at rotational speeds ranging from 10 to 100 rpm [50]

**Drug Content**

The amount of drug concentration was quantified by dissolving 0.1 g portion of the gel in 5 mL of methanol, followed by analysis using an established by UV–visible spectrophotometric technique at 255.60 nm (y = 0.021x + 0.0107, $R^2$ = 0.9974). the drug content was calculated using a standard calibration curve value [50].

$$\text{Concentration of sample} = \frac{Absorbance\ of\ sample}{Absorbance\ of\ standard} \times \frac{Concentration\ of\ standard}{Concentration\ of\ sample} \times 100$$

**Mucoadhesive strength**

Mucoadhesive strength was evaluated using freshly excised goat nasal mucosa obtained from a local slaughterhouse. The tissue was mounted on a glass slide, moistened with nasal saline buffer (pH 6.4), and 50 mg of microspheres were evenly applied. The slide was positioned at a 45° angle, and preheated nasal saline buffer (pH 6.4, 37 °C) was perfused dropwise at 1 mL/min for 1 hour using a peristaltic pump. After perfusion, 1 mL of the supernatant was collected, diluted, and analyzed by UV spectrophotometry to calculate % mucoadhesion using the following formula [51].

**Hemolytic Study**

Fresh blood was collected in anticoagulant tubes (EDTA) and centrifuged at 1500–2000 rpm for 10 minutes at 4 °C. Plasma and the buffy coat were discarded, and the red blood cell (RBC) pellet was rinsed three times with phosphate-buffered saline (pH 7.4). A 2% (v/v) RBC suspension was then prepared in PBS. For hemolysis evaluation, four test groups were prepared: saline (0.9% NaCl), distilled water, phosphate buffer (pH 7.4), reconstituted PLGA formulation, and pure tetrandrine. The PLGA formulation was centrifuged, the supernatant discarded, and the pellet reconstituted in PBS. Each test solution (5 mL) was mixed with RBC suspension and incubated 1 hour and then centrifuged at 3000 rpm for 10 minutes. The resulting supernatant was separated, diluted with PBS (pH 7.4), and its absorbance was determined at 540 nm using a UV–visible spectrophotometer, with saline serving as the reference [46].

***In- Vitro*Drug Release Study**

The drug release behavior of TET from the nanoparticles was assessed at pH 5.5 and 37 °C to mimic the tumor microenvironment. The nanoparticle suspension was loaded into dialysis membranes (MWCO 14,000 Da) and incubated in phosphate-buffered saline (PBS) with continuous magnetic stirring at 100 rpm. At every 1-hour interval, 2 mL of the dissolution medium was withdrawn and replacedwith an equivalentportion of fresh PBS. The collected samples were examined using UV spectrophotometry to calculate the cumulative percentage release of TET [52].

***Ex- Vivo* Diffusion Study**

*Ex vivo* permeationevaluation was carried out via Franz diffusion cell with freshly excised goat nasal mucosa procured from a nearby slaughterhouse. The mucosal tissue (1.77 $cm^2$) was rinsed, pre-equilibrated in phosphate buffer saline (PBS, pH 5.5) for 15 minutes, and positioned between the donor and receptor chambers. The receptor chamber (12 mL PBS, pH 5.5) was maintained at 34 °C under constant stirring at 400 rpm. An amount of0.3 mL of the nanoparticle preparation as loaded into the donor chamber, and 1 mL aliquots were collected from the receptor medium at predetermined hourly intervals, equally matched volumes of fresh PBS added to preserve maintaining sink conditions. The extracted samples were quantified using UV spectrophotometric analysis [52, 53].

**RESULTS AND DISCUSSION**

**Optimization of Formulation by Box-Behnken Design**

A total of 13 experimental runs including one center point were designed using the Box–Behnken approach to optimize PLGA nanoparticles with three independent and three dependent factors. The prepared nanoparticles were evaluated for various characteristics such as mean particle size, polydispersity index, zeta potential, and drug entrapment efficiency. The influence of

Journal of Chemical Health Risks

www.jchr.org

JCHR (2025) 15(5), 904-920 | ISSN:2251-6727

independent variables on the responses was analyzed, and corresponding 3D surface and contour plots were generated (Table 2).

**Table 2. Effect of Independent Variables on Dependent Variables**

| Batch | A:PLGA(mg) | B:Tween (%) | C:Stirring Time ( Hr) | Particle Size (nm) | Zeta Potential (mv) | Entrapment Efficiency (%) |
|---|---|---|---|---|---|---|
| **1** | 20 | 1 | 3 | 245.06 | -20.7 | 96.97 |
| **2** | 30 | 0.55 | 2 | 639.46 | -29.1 | 81.58 |
| **3** | 30 | 0.1 | 3 | 674.24 | -30.89 | 85.65 |
| **4** | 25 | 0.1 | 2 | 416.11 | -24.9 | 94.22 |
| **5** | 20 | 0.55 | 4 | 165.96 | -22.3 | 98.01 |
| **6** | 30 | 1 | 3 | 846.01 | -30.4 | 80.23 |
| **7** | 25 | 0.1 | 4 | 432.43 | -24.9 | 91.67 |
| **8** | 30 | 0.55 | 4 | 624.06 | -31.9 | 82.14 |
| **9** | 20 | 0.1 | 3 | 193.24 | -19.9 | 97.45 |
| **10** | 20 | 0.55 | 2 | 246.12 | -20.9 | 92.34 |
| **11** | 25 | 1 | 4 | 309.43 | -24.9 | 93.24 |
| **12** | 25 | 0.55 | 3 | 389.01 | -27.1 | 91.44 |
| **13** | 25 | 1 | 2 | 439.41 | -25.6 | 90.23 |

**Effect of Independent Parameters on Particle size**

The particle size of the prepared formulations varied significantly depending on the levels of PLGA, Tween, and stirring time as explored using the Design of Experiments (DoE) approach. The observed particle sizes ranged from approximately 165 nm to 846 nm across the different experimental runs. It was evident from the results that the amount of PLGA (A) had a pronounced effect on the particle size, with an increase in polymer concentration leading to larger particles. In contrast, the concentration of Tween (B) exhibited a comparatively minor influence, while stirring time (C) showed a slight negative correlation, suggesting that prolonged stirring may contribute to smaller particle sizes by promoting better dispersion.The mathematical model generated from the experimental data is described by the equation:

Particle size (nm) = 432.29 + 241.76A + 15.49B − 26.24C,

indicating that PLGA concentration is the most critical factor affecting particle size. The 3D surface and contour plots further corroborated these findings, illustrating that higher PLGA levels significantly increase particle dimensions, while variations in Tween and stirring time have a less dominant impact (figure 3).These results are in agreement with the expected behavior where polymer concentration directly affects particle formation, and surfactant presence and mechanical mixing parameters help to stabilize and reduce particle aggregation. The optimized conditions for achieving smaller particle size were found at lower polymer concentrations combined with adequate surfactant levels and stirring time, which are crucial for applications requiring efficient drug delivery and stability

Journal of Chemical Health Risks

www.jchr.org

JCHR (2025) 15(5), 904-920 | ISSN:2251-6727

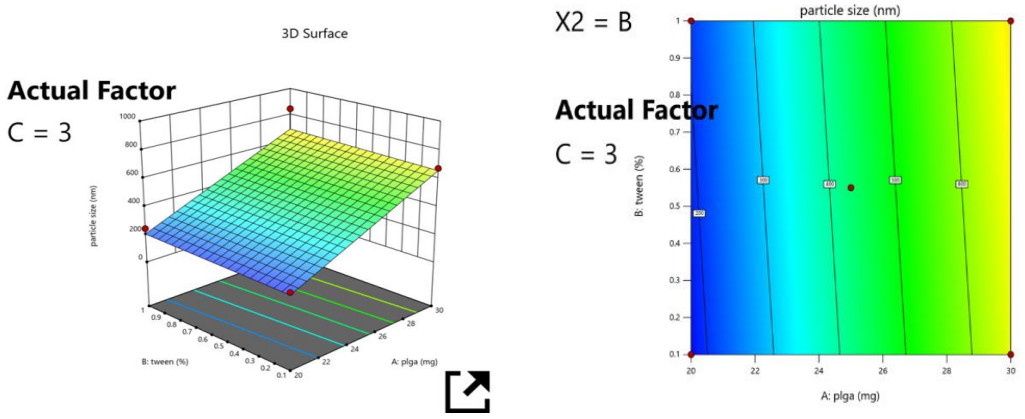


**Figure 3. 3D plot and Contour plot of particle size**

**Effectof Independent Parameters on Zeta Potential**

The zeta potential of the formulated nanoparticles was evaluated to understand the stability and surface charge characteristics of the particles under different formulation conditions. The observed zeta potential values ranged from −19.9 mV to −31.9 mV across various experimental runs. The mathematical model obtained from the experimental data is expressed as: Zeta Potential (mV) = −25.65 − 4.81A − 0.1262B − 0.4375C,

where A represents the amount of PLGA, B represents the concentration of Tween, and C represents the stirring time.The results indicated that an increase in the PLGA concentration led to a more negative zeta potential, suggesting that higher polymer amounts contribute to greater surface charge and enhanced particle stability. The influence of Tween concentration and stirring time was found to be less significant, although both factors showed a slight negative correlation with zeta potential. The 3D surface and contour plots further highlighted that the zeta potential decreased as PLGA concentration increased, while variations in surfactant concentration and stirring duration had comparatively minor effects.The negative values of zeta potential observed throughout the study suggest sufficient repulsive forces between particles, which can prevent aggregation and contribute to colloidal stability (figure 4). Formulations with higher absolute zeta potential values are expected to be more stable during storage and in physiological conditions. Therefore, optimizing the formulation parameters, particularly the PLGA concentration, is essential to achieve nanoparticles with favorable surface characteristics for targeted drug delivery.

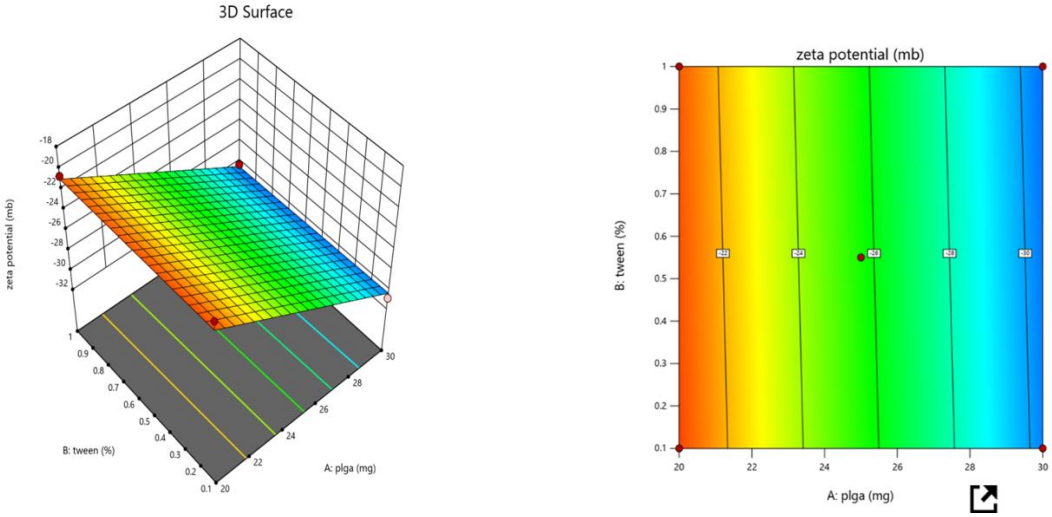


**Figure 4- 3D Graph and Contour plot of Zeta potential**

Journal of Chemical Health Risks

www.jchr.org

JCHR (2025) 15(5), 904-920 | ISSN:2251-6727

**Effectof Independent Parameters on Entrapment Efficiency (EE%)**

Entrapment efficiency (EE) of nanoparticles was analyzed using Box–Behnken Design (BBD), examining the effects of PLGA concentration (A), Tween 80 concentration (B), and stirring time (C). The relationship was modeled by the equation: EE (%) = 90.40 – 6.90A – 1.04B + 0.8362C. PLGA concentration significantly decreased EE due to increased viscosity and polymer saturation. Tween 80 also reduced EE, likely by lowering interfacial tension and promoting drug partitioning into the aqueous phase. Stirring time positively impacted EE by enhancing emulsification and nanoparticle stability. Response surface plots confirmed these trends (figure 5), showing EE decreased with higher PLGA and Tween 80 concentrations and improved with increased stirring. Experimental EE values ranged from 80–96%, indicating efficient drug loading suitable for nasal-to-brain delivery.

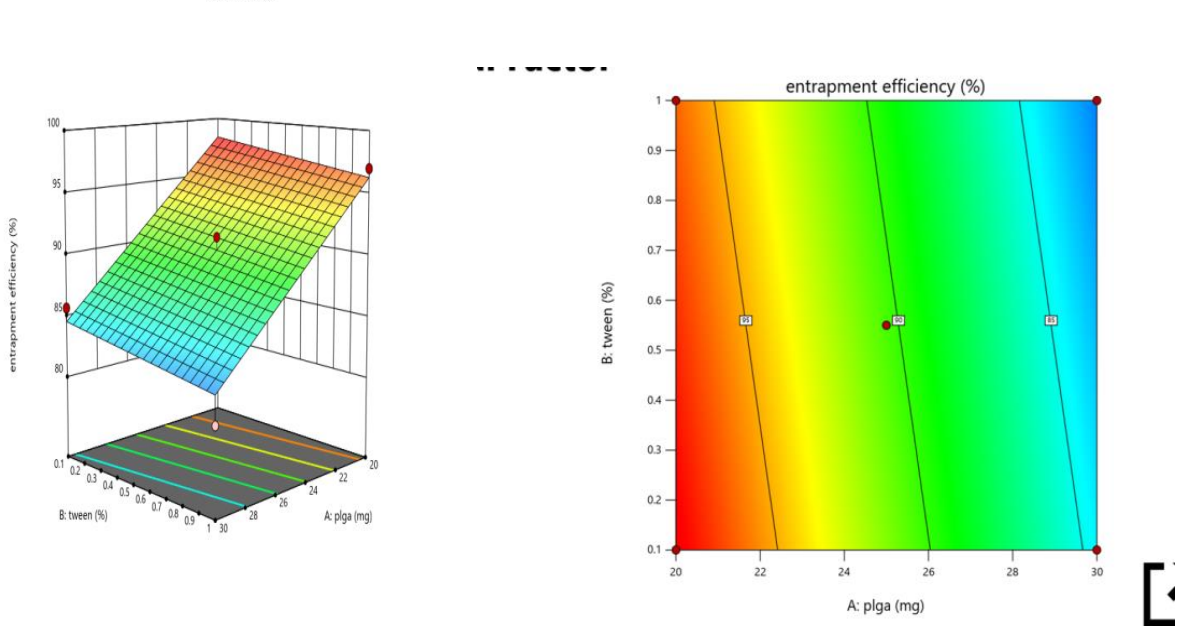


**Figure5- 3D Graph and Contour plot of Entrapment efficiency**

**Characterization of Tetrandrine-PLGA nanoparticles**

**Particle size**

The particle size distribution of the optimized formulation showed a narrow and uniform peak, indicating a well-dispersed nanoparticle system. The particle sizes ranged around **165.5 nm**, (figure 6) reflecting consistent formation with minimal aggregation. Such a controlled size distribution is important for enhancing stability, drug delivery efficiency, and cellular uptake, making the nanoparticles suitable for therapeutic applications.

**Zeta Potential**

The zeta potential distribution of the optimized nanoparticle formulation showed a single, sharp peak centered at **−22.3 mV**(figure 7), indicating a stable dispersion with sufficient surface charge to prevent aggregation. The narrow distribution suggests uniform particle behavior, which is essential for maintaining colloidal stability and enhancing the formulation's performance in drug delivery applications.

Journal of Chemical Health Risks
www.jchr.org
JCHR (2025) 15(5), 904-920 | ISSN:2251-6727

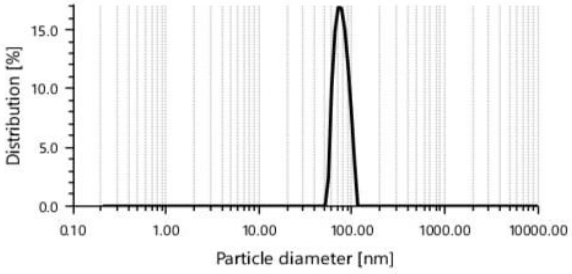


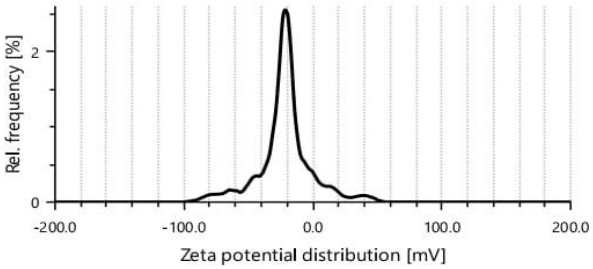


**Figure 6. Graph of Particle sizeFigure 7. Graph of Zeta Potential**

**FTIR Spectral Analysis**

FTIR analysis confirmed the successful encapsulation of Tetrandrine (TET) within PLGA nanoparticles without significant drug-polymer interactions. Characteristic peaks of pure TET (figure 8), corresponding to O–H/N–H, C–H, and C=C stretching, were present in the nanoparticle spectrum (figure 9), indicating TET's structural integrity. The nanoparticle spectrum also showed peaks attributable to the PLGA polymer, specifically at 1749.4 $cm^{-1}$ (C=O ester) and between 1230–1070 $cm^{-1}$ (ether/ester vibrations). These findings validate the compatibility of TET with PLGA, a crucial factor for stable and effective drug delivery.

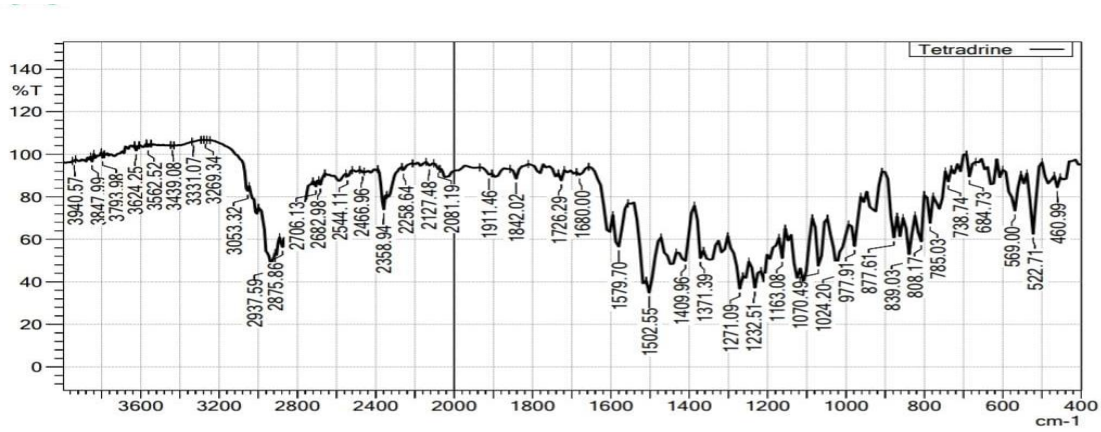


**Figure8. FTIR Spectrum of Tetrandrine**

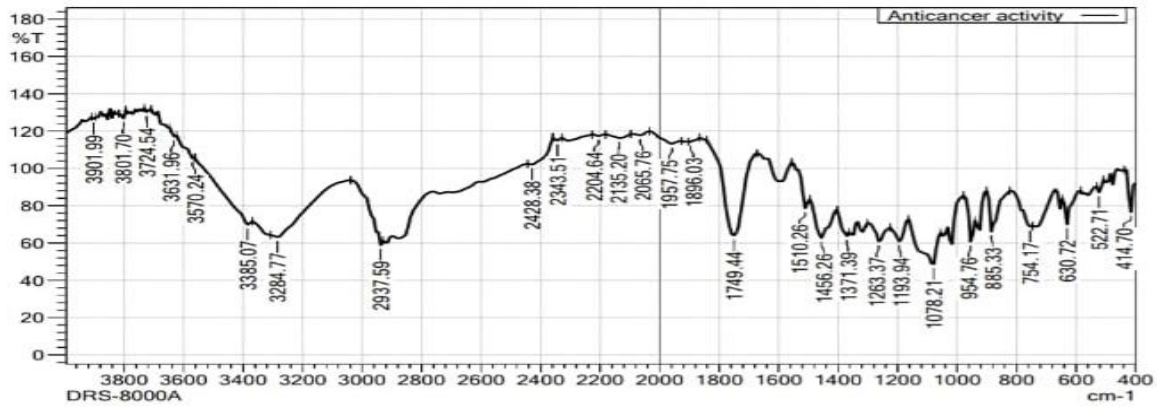


**Figure 9. FTIR Spectrum of Tetrandrine loaded Nanoparticles**

Journal of Chemical Health Risks

www.jchr.org

JCHR (2025) 15(5), 904-920 | ISSN:2251-6727

**Differential Scanning Calorimetry (DSC)**

Differential Scanning Calorimetry thermograph revealed that pure TET (figure 10) has a sharp melting endotherm at 222.4°C, indicating high crystallinity. TET-loaded PLGA (figure 11) nanoparticles exhibited a broadened peak at a lower temperature (161.07°C), signifying reduced crystallinity and a depression in melting point. This suggests TET is molecularly dispersed or amorphous within the PLGA matrix, which is advantageous for improving solubility and dissolution rates, potentially enhancing bioavailability. The DSC results confirm successful TET encapsulation in PLGA nanoparticles and demonstrate the formulation's capacity to improve TET's solubility.

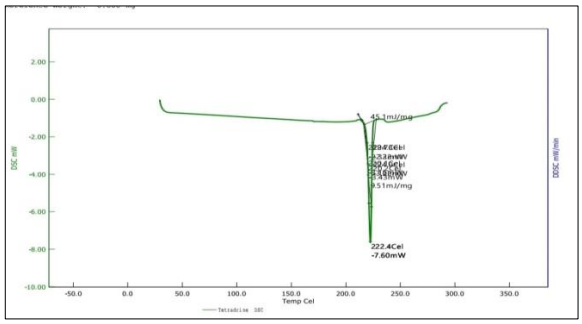


**Figure 10. DSC Thermogram ofTetrandrine**

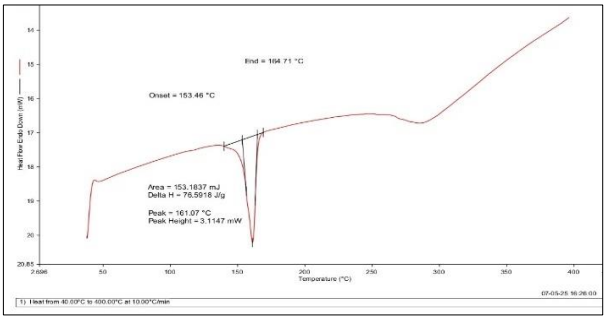


**Figure 11. DSC Thermogram of PLGA Tetrandrine Nanoparticles**

**X-Ray Diffraction (XRD) Analysis**

XRD analysis of pure Tetrandrine (figure 12) revealed sharp, intense peaks (2θ = 10°–35°) indicative of a highly crystalline structure, typically associated with poor aqueous solubility and low bioavailability. In contrast, Tetrandrine-loaded PLGA nanoparticles (figure 13) exhibited broader, less intense peaks and a broad background hump (40°–60°), signifying a reduction in crystallinity and the development of partial amorphous character. This transformation, confirmed by peak broadening consistent with nanometer-scale crystallite reduction via Scherrer equation analysis, suggests Tetrandrine was molecularly dispersed within the PLGA matrix. The shift from crystalline to partially amorphous form is beneficial for drug delivery, promoting higher free energy, improved wettability, enhanced dissolution rates, and increased bioavailability. The XRD results (figure 14) thus confirm successful reduction of Tetrandrine crystallinity and induction of amorphous character by PLGA nanoparticle encapsulation, leading to improved pharmaceutical performance.

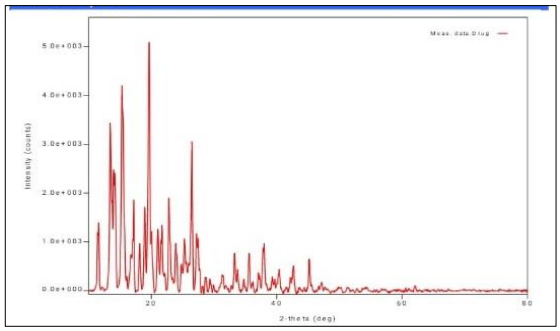


**Figure 12. XRD graph of Tetrandrine**

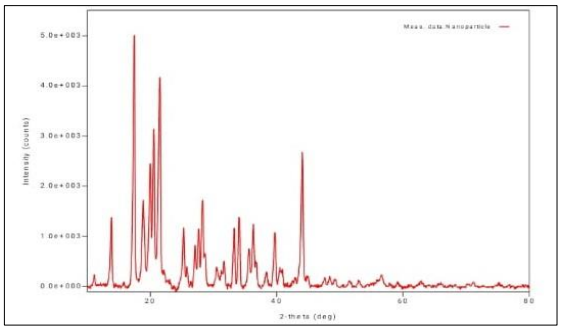


**Figure 13. XRD graph of Tetrandrine-PLGA Nanoparticles**

Journal of Chemical Health Risks

www.jchr.org

JCHR (2025) 15(5), 904-920 | ISSN:2251-6727

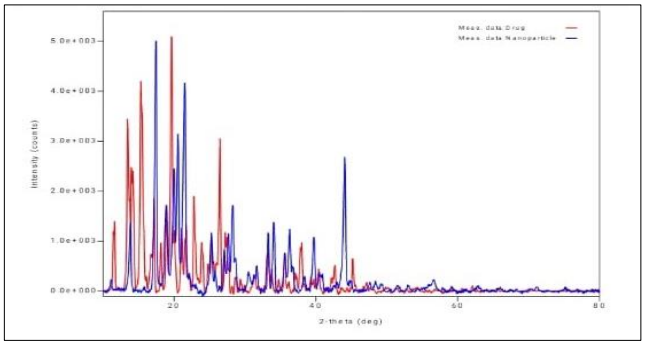


**Figure 14. XRD Overlay graph of Tetrandrine and Nanoparticles**

**Surface Morphology by FESEM**

FESEM analysis revealed Tetrandrine-loaded PLGA nanoparticles (figure 15) as spherical to near-spherical, smooth, and minimally aggregated, with sizes of 110–122 nm, suitable for nasal-to-brain delivery. The smooth surface indicates a stable formulation, while the lack of fused or irregular particles highlights the effectiveness of Tween 80 stabilization and optimized stirring in the preparation process.

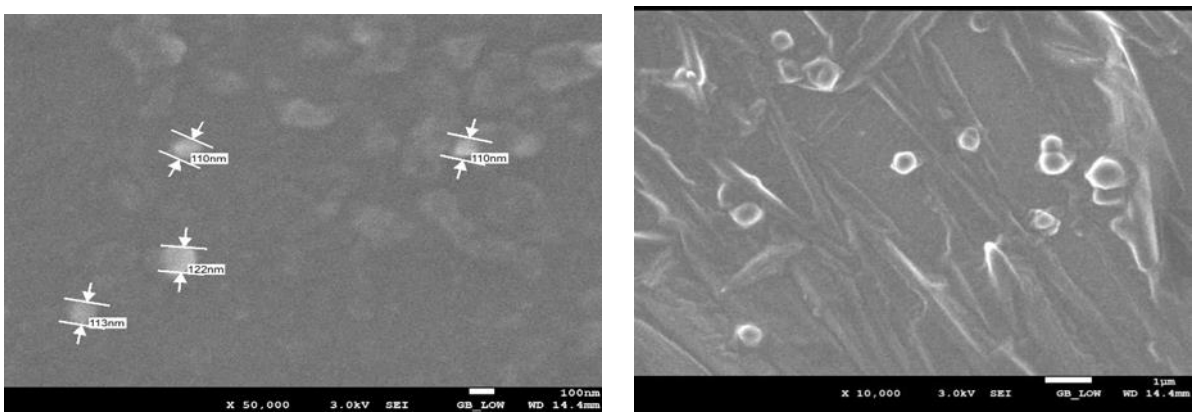


**Figure 15. FESEM of Tetrandrine-PLGA Nanoparticles**

**Evaluation of *In Situ* gel formulation.**

All formulations exhibited excellent clarity, with no visible particulate matter, essential for patient acceptance in ocular and mucosal applications. Their pH values ranged from 5.6 to 6.0, which is physiologically compatible with the ocular mucosa, minimizing irritation and ensuring stability. The formulations demonstrated rapid sol-to-gel transitions near physiological temperatures, with gelling times between 15.0-20.3 seconds and gelation temperatures between 35.1-36.8 °C, suitable for in situ gelling applications. Viscosity increased significantly from a sol state (128.12-280.32 cP) to a gel state (3010.89-6678.89 cP), with the higher gel viscosity aiding drug retention and the lower sol viscosity facilitating administration. Spreadability values of 9.2-10.3 cm indicated adequate uniformity of application. The drug content was 93.95%, reflecting efficient incorporation into the gel matrix.

**Drug Content**

The study found that PLGA nanoparticle-loaded in situ gel demonstrated significantly higher drug loading efficiency (84.76%) compared to the in situ gel alone (48.49%), due to the nanoparticles' encapsulation capabilities which also suggest improved sustained release. The prepared in situ gels possess favorable physicochemical properties including suitable clarity, pH, rapid gelation at physiological temperatures, optimal viscosity, adequate spread ability, high drug content, and strong mucoadhesion, making them appropriate for sustained, localized drug delivery.

Journal of Chemical Health Risks

www.jchr.org

JCHR (2025) 15(5), 904-920 | ISSN:2251-6727

**Mucoadhesion Study**

The mucoadhesive properties of the formulations were evaluated by measuring the amount of drug washed off from the mucosal surface. The Tetrandrine-loaded in situ gel exhibited a mucoadhesion of 48.49%, whereas the PLGA nanoparticles-loaded in situ gel showed a significantly higher mucoadhesion of 84.76% (table 3). This improvement can be attributed to the presence of nanoparticles, which enhance the interaction with mucosal tissues and increase retention time. The results suggest that incorporating PLGA nanoparticles into the gel matrix significantly strengthens the mucoadhesive behavior, potentially improving drug absorption and therapeutic efficacy.

**Table3.Mucoadhesion Study of *In - Situ* Gel**

| **Formulation** | **Drug Loaded (mg)** | **Absorbance** | **Drug Washed Off (mg)** | **% Mucoadhesion** |
|---|---|---|---|---|
| Tetrandrine-loaded *In Situ* Gel | 2.00 | 0.1860 | 1.03 | **48.49%** |
| Tetrandrine - PLGA Nanoparticles-loaded *In Situ* Gel | 4.00 | 0.1109 | 0.61 | **84.76%** |

**Hemolytic Activity Evaluation**

The nano formulation exhibited 21.6% hemolysis, a lower rate than the free drug (69%) and a positive control (80% distilled water), but higher than a negative control (5% physiological buffer). Microscopic analysis showed minimal disruption from the nano formulation compared to severe lysis caused by the free drug and distilled water. This reduced hemolytic activity is attributed to PLGA encapsulation limiting direct drug-membrane interaction. However, the 21.6% hemolysis exceeds the ASTM E2524-08 threshold (<10%), suggesting a need for surface modifications like PEGylation for improved hemocompatibility (table 4). The nano formulation significantly improves biocompatibility and reduces RBC toxicity compared to the free drug, indicating potential for systemic or nasal anticancer delivery, pending further optimization for clinical use.

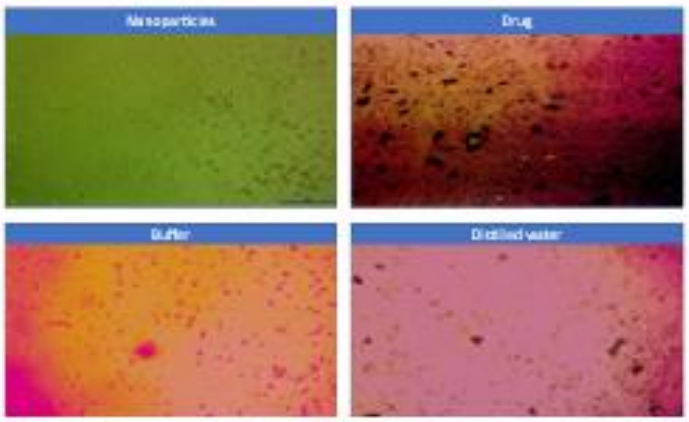


**Figure 16. Microscopic Images of Hemolytic Study**

**Table 4.Hemolysis percentage and RBC morphology observations**

| **Groups** | **% Hemolysis (Mean ± SD)** | **Microscopy Findings (40×)** | **Interpretation** |
|---|---|---|---|
| **Physiological buffer (Negative control)** | 5% (baseline) | Normal biconcave RBCs; intact membranes | Safe, non-hemolytic |

Journal of Chemical Health Risks

www.jchr.org

JCHR (2025) 15(5), 904-920 | ISSN:2251-6727

| | | | |
|---|---|---|---|
| **Distilled water (Positive control)** | 80% | Complete RBC lysis; severe morphological damage | Maximum hemolysis due to osmotic rupture |
| **Free drug** | 69% | Severe RBC lysis; distorted cell morphology | High membrane toxicity |
| **Nano formulation (PLGA-based)** | 21.6% | Minimal disruption; mostly intact RBC morphology | Reduced hemolysis vs drug, but >10% threshold |

### *In - Vitro* Drug Release Profile

Drug release profiles for NP, D-ISG, and NP-ISG were assessed over 72 hours. NP-ISG demonstrated the slowest initial release (0-6h) and the slowest overall release (82% by 72h), attributed to dual control from nanoparticle encapsulation and a gel barrier. D-ISG showed slightly faster initial release and the highest cumulative release (97%) by 72 hours, while NP exhibited moderate and steady release (90% by 72h) (figure17). All formulations showed minimized burst release due to gel incorporation. NP-ISG's prolonged release profile is beneficial for reducing dosing frequency and maintaining therapeutic levels, making it suitable for nasal-to-brain delivery in glioblastoma therapy.

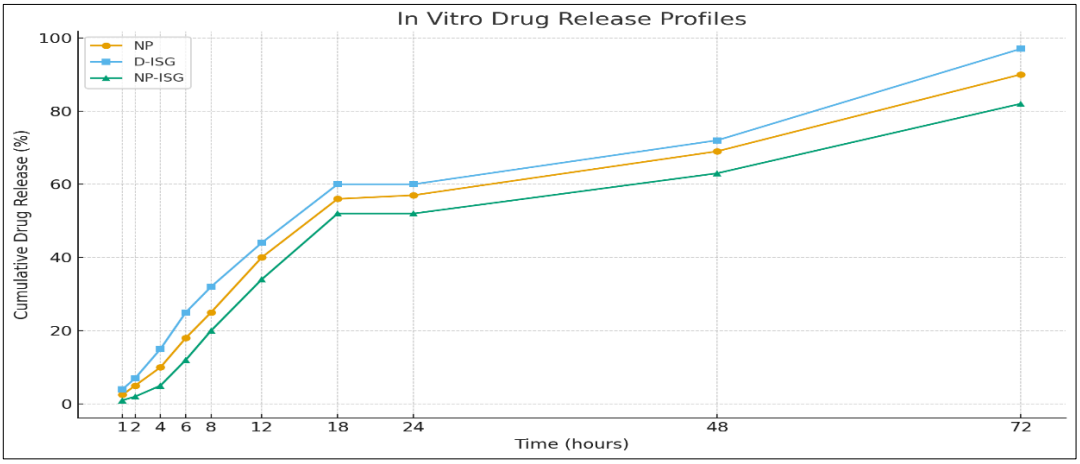


**Figure 17. *In - vitro*Drug Release Study**

### *Ex Vivo*Drug Release

A drug release and external biological environment study compared Nanoparticles (NP), Drug-loaded In situ gel (D-ISG), and Nanoparticles-loaded In situ gel (NP-ISG) over 72 hours. Initial release (<5% in 2h) was minimal for all, with D-ISG slightly higher. NP-ISG showed the slowest release due to the gel barrier. Between 6-12 hours, NP-ISG release significantly increased due to gel erosion, surpassing other formulations by 12 hours. By 24 hours, all formulations reached approximately 50% cumulative release. At 72 hours, D-ISG (89.64%) and NP (85.81%) showed higher cumulative release than NP-ISG (81.53%) (figure 18), confirming NP-ISG's prolonged and controlled release profile. NP-ISG is considered suitable for nasal-to-brain delivery due to its dual-controlled release mechanism.

Journal of Chemical Health Risks

www.jchr.org

JCHR (2025) 15(5), 904-920 | ISSN:2251-6727

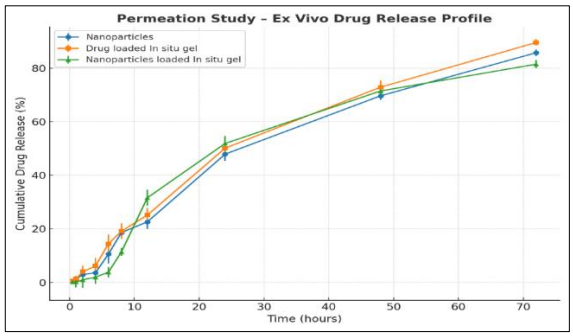


**Figure 18.*Ex - Vivo* Drug Release Profile**

## CONCLUSION

In this research, Tetrandrine-loaded PLGA nanoparticles incorporated into an in situ gel system were successfully developed and characterized to enhance brain-targeted drug delivery. The optimized formulation exhibited a particle size of 165.5 nm, which is ideal for efficient permeation and cellular uptake, and a zeta potential of −22.3 mV, indicating good colloidal stability. The formulation also demonstrated suitable pH, gelation temperature, and viscosity, ensuring ease of application and rapid gel formation under physiological conditions. The mucoadhesive strength was significantly improved in the nanoparticle-based gel (~84.76%) compared to the free drug (~48.49%), suggesting better adhesion to mucosal surfaces and prolonged residence time. Hemolysis studies confirmed the safety profile, showing minimal membrane disruption and lower toxicity than the free drug. In vitro and ex vivo release studies further highlighted the controlled and sustained release behavior of the NP-ISG system over 72 hours, reducing initial burst release and providing a steady therapeutic effect.

These findings indicate that the nanoparticle-loaded in situ gel holds substantial promise for delivering Tetrandrine effectively across biological barriers, especially for the treatment of glioblastoma and other brain-related disorders. In future work, this delivery system could be further optimized for targeted brain delivery through nasal routes and tested in relevant animal models to assess pharmacokinetics, biodistribution, and therapeutic efficacy. Additionally, exploring its application with other hydrophobic or poorly soluble drugs could expand its utility across various clinical scenarios. Overall, this study lays a solid foundation for the development of safer, more efficient, and patient-compliant drug delivery systems aimed at improving outcomes in neurological disorders.

## DECLARATIONS

**Ethical Approval:** NA

**Consent to Participate:** NA

**Consent for publication:** NA

**Availability of Supporting Data:** No Data

**Competing Interest:** NA

**Funding:** NA

## REFERENCES

1. Jiang Y., et al. *History of uses, phytochemistry, pharmacological activities, quality control and toxicity of the root of Stephania tetrandra S. Moore: A review.* J Ethnopharmacol. 2020;259:112934.
2. Zhao Z., et al. *A critical review: traditional uses, phytochemistry, pharmacology and toxicology of Stephania tetrandra S. Moore (Fen Fang Ji).* Phytochem Rev. 2020;19:1449–1476.
3. Sun Y., et al. *Tetrandrine: a review of its anticancer effects and underlying mechanisms.* Front Pharmacol. 2022;13:896050.
4. Yu S., et al. *Pharmacological effects of tetrandrine and fangchinoline: bisbenzylisoquinoline alkaloids from Stephania tetrandra.* Pharmacol Res. 2020;161:105164.
5. Chen Y., et al. *Tetrandrine, a calcium channel blocker: pharmacological and clinical aspects.* Phytother Res. 2018;32(1):3–22.
6. Liu Y., et al. *Bisbenzylisoquinoline alkaloids from Stephania tetrandra and their pharmacological activities.* Fitoterapia. 2019;137:104262.
7. He L., et al. *Tetrandrine induces cell cycle arrest and apoptosis in human colon cancer cells.* Cancer Chemother Pharmacol. 2002;49:261–266.
8. Zhang Y., et al. *Tetrandrine induces mitochondria-mediated apoptosis in gastric cancer cells.* Biochem Biophys Res Commun. 2012;425:615–620.

9. Wang H.Q., et al. *Tetrandrine triggers autophagy through suppression of the PI3K/AKT/mTOR pathway in breast cancer cells.* Int J Oncol. 2011;39:1319–1326.

10. He L., et al. *Cell cycle arrest in G1 phase induced by tetrandrine in colon cancer cells.* Cancer Chemother Pharmacol. 2002;49:261–266.

11. Zhang Y., et al. *Mitochondria-mediated apoptosis induced by tetrandrine in human gastric cancer BGC-823 cells.* Biochem Biophys Res Commun. 2012;425:615–620.

12. Wang H.Q., et al. *Autophagy induction by tetrandrine through inhibition of PI3K/AKT/mTOR pathway in breast cancer cells.* Int J Oncol. 2011;39:1319–1326.

13. Xu W., et al. *Tetrandrine suppresses migration and invasion of colon cancer SW620 cells via NF-κB/MMP signaling.* Biomed Pharmacother. 2018;101:945–951.

14. Zhang L., et al. *Tetrandrine suppresses glioma angiogenesis and growth in vivo.* Cancer Lett. 2011;301:21–31.

15. Wang J., et al. *Anti-glioma effects of tetrandrine: suppression of angiogenesis and tumor growth in rats.* Oncol Rep. 2012;28:1259–1266.

16. Tsuruo T., et al. *Reversal of multidrug resistance by bisbenzylisoquinoline alkaloids, tetrandrine and fangchinoline.* Cancer Res. 1984;44:4303–4307.

17. Wu C.P., et al. *Tetrandrine potentiates anticancer drug transport across the blood–brain barrier by inhibiting P-glycoprotein.* Cancer Chemother Pharmacol. 2011;68:957–969.

18. Pan G.Y., et al. *Pharmacokinetics and BBB penetration of tetrandrine in rats.* Planta Med. 2010;76(17):1804–1809.

19. Yu X., et al. *Tetrandrine and its potential in treating multidrug-resistant cancers.* Drug Des Devel Ther. 2020;14:1707–1720.

20. Bhagya NC, Chandrashekar KR. Tetrandrine and cancer–An overview on the molecular approach. Biomedicine & Pharmacotherapy. 2018 Jan 1;97:624-32.

21. Bhagya N, Chandrashekar KR. Autophagy and cancer: Can tetrandrine be a potent anticancer drug in the near future?. Biomedicine & Pharmacotherapy= Biomedecine & Pharmacotherapie. 2022 Feb 24;148:112727-.

22. Grochans S, Cybulska AM, Simińska D, Korbecki J, Kojder K, Chlubek D, Baranowska-Bosiacka I. Epidemiology of glioblastoma multiforme–literature review. Cancers. 2022 May 13;14(10):2412.

23. Sai K, Yang QY, Shen D, Chen ZP. Chemotherapy for gliomas in mainland China: an overview. Oncology letters. 2013 May;5(5):1448-52.

24. Li X, Lu X, Xu H, Zhu Z, Yin H, Qian X, Li R, Jiang X, Liu B. Paclitaxel/tetrandrine coloaded nanoparticles effectively promote the apoptosis of gastric cancer cells based on “oxidation therapy”. Molecular pharmaceutics. 2012 Feb 6;9(2):222-9.

25. Yoo SM, Oh SH, Lee SJ, Lee BW, Ko WG, Moon CK, Lee BH. Inhibition of proliferation and induction of apoptosis by tetrandrine in HepG2 cells. Journal of ethnopharmacology. 2002 Jul 1;81(2):225-9.

26. Kuo PL, Lin CC. Tetrandrine-induced cell cycle arrest and apoptosis in Hep G2 cells. Life sciences. 2003 May 30;73(2):243-52.

27. Oh SH, Lee BH. Induction of apoptosis in human hepatoblastoma cells by tetrandrine via caspase-dependent Bid cleavage and cytochrome c release. Biochemical pharmacology. 2003 Sep 1;66(5):725-31.

28. Chen Y, Tseng SH. The potential of tetrandrine against gliomas. Anti-Cancer Agents in Medicinal Chemistry (Formerly Current Medicinal Chemistry-Anti-Cancer Agents). 2010 Sep 1;10(7):534-42.

29. Chen Y, Chen JC, Tseng SH. Tetrandrine suppresses tumor growth and angiogenesis of gliomas in rats. International journal of cancer. 2009 May 15;124(10):2260-9.

30. Alghareeb S, Asare-Addo K, Conway BR, Adebisi AO. PLGA nanoparticles for nasal drug delivery.

Journal of Drug Delivery Science and Technology. 2024 May 1;95:105564.

31. Pandey A, Jain DS. Poly Lactic-Co-Glycolic Acid (PLGA) copolymer and its pharmaceutical application. Handbook of polymers for pharmaceutical technologies: processing and applications. 2015 Aug 10;2:151-72.
32. Wu XS, Wang N. Synthesis, characterization, biodegradation, and drug delivery application of biodegradable lactic/glycolic acid polymers. Part II: biodegradation. Journal of Biomaterials Science, Polymer Edition. 2001 Jan 1;12(1):21-34.
33. Swider, Edyta, et al. "Customizing poly (lactic-co-glycolic acid) particles for biomedical applications." *Acta biomaterialia* 73 (2018): 38-51.
34. Abu Ammar A, Nasereddin A, Ereqat S, Dan-Goor M, Jaffe CL, Zussman E, Abdeen Z. Amphotericin B-loaded nanoparticles for local treatment of cutaneous leishmaniasis. Drug delivery and Translational research. 2019 Feb 15;9(1):76-84.
35. Abu Ammar A, Raveendran R, Gibson D, Nassar T, Benita S. A lipophilic Pt (IV) oxaliplatin derivative enhances antitumor activity. Journal of medicinal chemistry. 2016 Oct 13;59(19):9035-46.
36. Huang W, Zhang C. Tuning the size of poly (lactic-co-glycolic acid)(PLGA) nanoparticles fabricated by nanoprecipitation. Biotechnology journal. 2018 Jan;13(1):1700203.
37. Iqbal M, Zafar N, Fessi H, Elaissari A. Double emulsion solvent evaporation techniques used for drug encapsulation. International journal of pharmaceutics. 2015 Dec 30;496(2):173-90.
38. Waghule T, Rapalli VK, Singhvi G, Manchanda P, Hans N, Dubey SK, Hasnain MS, Nayak AK. Voriconazole loaded nanostructured lipid carriers based topical delivery system: QbD based designing, characterization, in-vitro and ex-vivo evaluation. Journal of drug delivery science and technology. 2019 Aug 1;52:303-15.
39. Bhanderi M, Shah J, Gorain B, Nair AB, Jacob S, Asdaq SM, Fattepur S, Alamri AS, Alsanie WF, Alhomrani M, Nagaraja S. Optimized rivastigmine nanoparticles coated with eudragit for intranasal application to brain delivery: evaluation and nasal ciliotoxicity studies. Materials. 2021 Oct 22;14(21):6291.
40. Dilawar N, Ur-Rehman T, Shah KU, Fatima H, Alhodaib A. Development and evaluation of PLGA nanoparticle-loaded organogel for the transdermal delivery of risperidone. Gels. 2022 Nov 2;8(11):709.
41. Kumbhar SA, Kokare CR, Shrivastava B, Gorain B, Choudhury H. Preparation, characterization, and optimization of asenapine maleate mucoadhesive nanoemulsion using Box-Behnken design: In vitro and in vivo studies for brain targeting. International journal of pharmaceutics. 2020 Aug 30;586:119499.
42. Waghule T, Rapalli VK, Singhvi G, Manchanda P, Hans N, Dubey SK, Hasnain MS, Nayak AK. Voriconazole loaded nanostructured lipid carriers based topical delivery system: QbD based designing, characterization, in-vitro and ex-vivo evaluation. Journal of drug delivery science and technology. 2019 Aug 1;52:303-15.
43. Gaba B, Fazil M, Khan S, Ali A, Baboota S, Ali J. Nanostructured lipid carrier system for topical delivery of terbinafine hydrochloride. Bulletin of Faculty of Pharmacy, Cairo University. 2015 Dec 1;53(2):147-59.
44. Che Marzuki NH, Wahab RA, Abdul Hamid M. An overview of nanoemulsion: concepts of development and cosmeceutical applications. Biotechnology & biotechnological equipment. 2019 Jan 1;33(1):779-97.
45. Chong WT, Tan CP, Cheah YK, B. Lajis AF, Habi Mat Dian NL, Kanagaratnam S, Lai OM. Optimization of process parameters in preparation of tocotrienol-rich red palm oil-based nanoemulsion stabilized by Tween80-Span 80 using response surface methodology. PLoS One. 2018 Aug 24;13(8):e0202771.
46. Singh N, Sahoo SK, Kumar R. Hemolysis tendency of anticancer nanoparticles changes with type of blood group antigen: An insight into blood nanoparticle interactions. Materials Science and Engineering: C. 2020 Apr 1;109:110645.

47. Pokharkar V, Patil-Gadhe A, Palla P. Efavirenz loaded nanostructured lipid carrier engineered for brain targeting through intranasal route: In-vivo pharmacokinetic and toxicity study. Biomedicine & pharmacotherapy. 2017 Oct 1;94:150-64.

48. Bondre RM, Kanojiya PS, Wadetwar RN, Kangali PS. Sustained vaginal delivery of in situ gel containing Voriconazole nanostructured lipid carrier: formulation, in vitro and ex vivo evaluation. Journal of Dispersion Science and Technology. 2023 Jun 23;44(8):1466-78.

49. Osmani RA, Kulkarni PK, Shanmuganathan S, Hani U, Srivastava A, Shinde CG, Bhosale RR. A 3 2 full factorial design for development and characterization of a nanosponge-based intravaginal in situ gelling system for vulvovaginal candidiasis. RSC advances. 2016;6(23):18737-50.

50. Choudhury H, Gorain B, Pandey M, Khurana RK, Kesharwani P. Strategizing biodegradable polymeric nanoparticles to cross the biological barriers for cancer targeting. International journal of pharmaceutics. 2019 Jun 30;565:509-22.

51. Choudhury H, Zakaria NF, Tilang PA, Tzeyung AS, Pandey M, Chatterjee B, Alhakamy NA, Bhattamishra SK, Kesharwani P, Gorain B, Md S. Formulation development and evaluation of rotigotine mucoadhesive nanoemulsion for intranasal delivery. Journal of Drug Delivery Science and Technology. 2019 Dec 1;54:101301.

52. Pardeshi CV, Belgamwar VS. Improved brain pharmacokinetics following intranasal administration of N, N, N-trimethyl chitosan tailored mucoadhesive NLCs. Materials Technology. 2020 Apr 15;35(5):249-66.

53. Gadhave DG, Kokare CR. Nanostructured lipid carriers engineered for intranasal delivery of teriflunomide in multiple sclerosis: optimization and in vivo studies. Drug development and industrial pharmacy. 2019 May 4;45(5):839-51.